

Band reduction for hyperspectral imagery processing

Stefan A. Robila*

Department of Computer Science, Center for Imaging and Optics, Montclair State University,
Montclair, NJ 07043

ABSTRACT


Feature reduction denotes the group of techniques that reduce high dimensional data to a smaller set of components. In remote sensing feature reduction is a preprocessing step to many algorithms intended as a way to reduce the computational complexity and get a better data representation. Reduction can be done by either identifying bands from the original subset (selection), or by employing various transforms that produce new features (extraction). Research has noted challenges in both directions. In feature selection, identifying an "ideal" spectral band subset is a hard problem as the number of bands is increasingly large, rendering any exhaustive search unfeasible. To counter this, various approaches have been proposed that combine a search algorithm with a criterion function. However, the main drawback of feature selection remains the rather narrow bandwidths covered by the selected bands resulting in possible information loss. In feature extraction, some of the most popular techniques include Principal Component Analysis, Independent Component Analysis, Orthogonal Subspace Projection, etc. While they have been used with success in some instances, the resulting bands lack a physical relationship to the data and are mostly produced using statistical strategies. We propose a new technique for feature reduction that exploits search strategies for feature selection to extract a set of spectral bands from a given imagery. The search strategy uses dynamic programming techniques to identify 'the best set' of features.

Keywords: feature extraction, hyperspectral imagery, search methods

1. INTRODUCTION

Remote sensing carries distinct advantages among the many scientific approaches used to measure and analyze: the ability to measure properties from the distance, without any contact with the phenomenon surveyed allows us to extract tremendous amounts of data on and yield answers to a wide array of problems. Among remote sensing techniques, photogrammetry is probably the first one introduced and determines geometric properties about objects from photographic images, in an effort to simulate and enhance human vision [1]. Based on progresses in color imaging, as an enhancement of photogrammetry, the last several decades have seen the development of various imaging sensors that no longer collect a single color or grayscale image but a collection of grayscale images (bands) each associated with an interval of spectrum wavelengths [2]. Such image is often called a multispectral image or dataset. Often a multispectral image contains one or more bands for each of the fundamental colors (blue, red, green) and includes bands for spectral regions not sensed by the human eye, such as infrared (see Table 1).

Table 1. Visible light spectrum.

	Color	Interval
	Violet	380–450 nm
	Blue	450–495 nm
	Green	495–570 nm
	Yellow	570–590 nm
	Orange	590–620 nm
	Red	620–750 nm

*robilas@mail.montclair.edu; phone 1 973 655-4230; fax 1 973 655-4164; pages.csam.montclair.edu/~robila

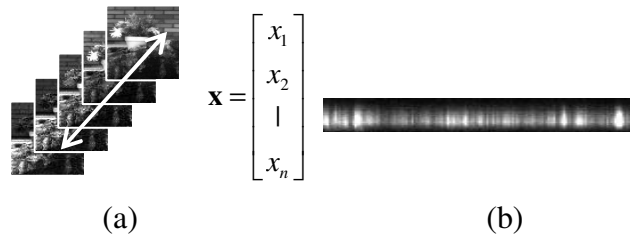


Figure 1. a) Spectra are formed of the pixel values for the same coordinates. b) A vertical slice through the data cube displaying variations among spectra

Building upon multispectral, hyperspectral sensors carry the distinctive advantage of recording hundreds of contiguous spectral images for the same scene providing an extraordinary amount of information that leads to precise differentiation of materials present in the scene even when such materials contribute only to few pixels [3]. With the advent of more and more powerful sensing platforms, coupled with reduction in manufacturing costs and diversification of technologies, hyperspectral imaging has become a powerful approach in remote sensing with applications spanning all traditional fields (such as agriculture, mining, military, resource management, etc.) as well as new ones (manufacturing quality control, pollution detection, health and life sciences, food safety etc.) [4,5]

Processing hyperspectral images centers on the concept of spectrum (see Fig 1). Current state of the art in spectral data processing aims of identifying materials present in the scene even when the spatial resolution of the sensor makes the material to occupy less than a pixel. Various models, both linear and nonlinear are used to express the idea of materials mixing within the pixel [4]. At the same time, most of the hyperspectral image processing techniques have complexity that depends directly on the number of spectral bands in the acquired data. Since this is usually large, it is of interest to find methods that transform the data cube into one with reduced dimensionality while, maintaining as much information content as possible. These techniques are known under the general name of feature reduction [6]. Feature extraction is done by either selecting certain bands (usually called selection) or by using a transform that produces the features as combinations of bands (also known as extraction). The algorithms focus on the increase of the separation between classes within each feature. The separation is measured using class information such as distance between spectra, means of spectra or statistical properties of the classes.

Recently, a new technique was introduced to enhance the separation of spectra by iteratively selecting the bands that increase the distance between spectra [7]. While not optimal, the approach was shown to match closely the results of an exhaustive run on a reduced dataset and also improve the classification accuracy for various images. The method is pursuing a forward direction only in the sense that once a band is selected, it will never be eliminated. We propose a dynamic selection algorithm that allows for both addition and elimination of bands based on general distance criteria. The method, based on floating feature selection [8] is then expanded to spectra classes for target discrimination.

The rest of the paper is organized as follows. In the second section we provide a short overview of the Best Angle (BA) algorithm introduced in [7]. We follow with our proposed generalized BA algorithm and provide experimental results. The paper ends with a brief conclusion, acknowledgements and references.

2. BEST ANGLE ALGORITHMS

In hyperspectral data the idea of spectra separability is at the basis of many problems. If a material spectrum is easily separable from the background, then the material will be easily detected in the image . If two adjoining materials have significantly dissimilar spectra, then the edge between them will also be easily detected. Unfortunately, clear separability cannot be easily achieved. Each spectrum is formed of tens to hundreds of values collected within narrow adjacent wavelength intervals and often exposes strong local correlation. Solutions to target separability are often found in the literature. One such popular distance is the spectral angle.

Given two vectors of the same dimension \mathbf{x} and \mathbf{y} , the *spectral angle* between them is defined as the arccosine of their dot product [9,10]:

$$SA(\mathbf{x}, \mathbf{y}) = \arccos \left(\frac{\langle \mathbf{x}, \mathbf{y} \rangle}{\|\mathbf{x}\| \|\mathbf{y}\|} \right) \quad (1)$$

where $\langle \cdot, \cdot \rangle$ represents the dot product of the vectors and $\|\cdot\|$ the Euclidean norm.

Since many of the vector components are strongly related to each other, it is of interest to design methods that selects only those bands that increase (or decrease the separability). Given two spectra \mathbf{x} and \mathbf{y} with values over a set of spectra bands \mathbf{B} , a spectral distance β the goal of band screening is to find the subset of bands \mathbf{B}_1 such that:

$$d(x, y, B_1) = \min_{B_1 \subseteq B} (d(x, y, B)) \quad (2)$$

where by $d(\mathbf{x}, \mathbf{y}, \mathbf{B}_s)$ we refer to the value of the distance measure β computed between the two vectors but taking into consideration only the bands included in the subset \mathbf{B}_s .

While finding the optimum subset is always possible through exhaustive search, the complexity of such operation is prohibitive. Given a hyperspectral image of n bands, and assuming the B_1 can have any size (between 2 and 210), the number of band combinations to be tried is roughly equivalent to the number of possible mappings:

$$f : \{1,2,3,\dots,n\} \rightarrow \{0,1\} \quad (3)$$

The above equation leads to 2^n possible mappings and is not solvable using regular computing environments [11]. In [7] a Best Angle (BA) algorithm was introduced. The algorithm is provided in short in Table 2. In the equations, \mathbf{x}_A denotes the vector $[x_{i1}, x_{i2}, x_{i3}, \dots]$ where $A=\{i1,i2,i3,\dots\}$. In other words it corresponds to the subvector of \mathbf{x} covering only the components found in A . The algorithms starts by finding two bands that would create the maximum distance between the corresponding subvectors. In proceeds to add additional bands as long as the distance increases. When this is no longer possible, the algorithm terminates.

The name of the algorithm (MAX) comes from the fact that it was designed such that the first step is focused on the maximum distance over two components. A complementary algorithm (MDM_MIN) was also introduced where Step 1 finds the two bands that span the minimum distance [7]. The algorithms are identified as Band Add-On (BAO) with Min and Max respectively, to reflect their additive approach. To help in the decision in steps 3 and 4, the spectral angle over B and j can be expressed as:

$$\cos(SA(\mathbf{x}_{[B_1,j]}, \mathbf{y}_{[B_1,j]})) = \cos(SA(\mathbf{x}_{B_1}, \mathbf{y}_{B_1})) \beta(\mathbf{x}, \mathbf{y}, B_1, j) \quad (4)$$

where:

$$\beta(\mathbf{x}, \mathbf{y}, B_1, j) = \frac{1 + \frac{\langle \mathbf{x}_j, \mathbf{y}_j \rangle}{\langle \mathbf{x}_{B_1}, \mathbf{y}_{B_1} \rangle}}{\sqrt{1 + \frac{\|\mathbf{x}_j\|^2}{\|\mathbf{x}_{B_1}\|^2}} \sqrt{1 + \frac{\|\mathbf{y}_j\|^2}{\|\mathbf{y}_{B_1}\|^2}}} \quad (5)$$

Table 2. BAO_MAX (Band Add-On – Maximum Initial Difference)

<p>Given two vectors \mathbf{x} and \mathbf{y} of size n</p> <p>Step 1. Find i and j between 1 and n with $[i, j] = \arg \max_{\substack{1 \leq k_1 \leq n \\ 1 \leq k_2 \leq n \\ k_1 \neq k_2}} d(\mathbf{x}_{[k_1, k_2]}, \mathbf{y}_{[k_1, k_2]})$</p> <p>Step 2. $B_1 = \{i, j\}$</p> <p>Step 3. Find k between 1 and n such that with $j = \arg \max_{k \notin B_1} d(\mathbf{x}_{[B_1, k]}, \mathbf{y}_{[B_1, k]})$</p> <p>Step 4. If $d(\mathbf{x}_{[B_1, j]}, \mathbf{y}_{[B_1, j]}) > d(\mathbf{x}_{B_1}, \mathbf{y}_{B_1})$</p> <p style="padding-left: 40px;">Step 5. Then $B_1 = B_1 \cup \{j\}$ and go to Step 3</p> <p style="padding-left: 40px;">Step 6. Else Stop.</p>
--

It can be shown that addition of band j will increase the angle only when the term $\beta(\mathbf{x}, \mathbf{y}, B_1, j)$ is smaller than 1. In that case BAO seeks the j that minimizes $\beta(\mathbf{x}, \mathbf{y}, B_1, j)$ as the candidate band to be added. The condition in Step 4 is replaced by a comparison of the $\beta(\mathbf{x}, \mathbf{y}, B_1, j)$ with 1.

A relatively extended suite of experiments and modifications for classification and target detection accompanied the introduction of the algorithm in [7]. They validated that the BAO algorithm is able to correctly discriminate pixels that were miss classified by other techniques. In parallel, the authors also showed that BAO is closely matching an optimal solution. However, the same experiments also showed significant difference between the MIN and MAX versions. Consistently, BAO_MAX provided the best results from the point of view of maximization of spectral angle, whereas BAO_MIN did not. In addition, the choice of the largest two band angle leads BAO_MAX to select only a very small number of bands (between 3 to 8), insufficient to express the variability within a class of spectra. The authors suggested the use of BAO_MIN in this case.

3. FLOATING BAND SELECTION

The drawback of the Band Add-On algorithm is the inability to backtrack at any step. In other words, once a band is added, the algorithm is unable to eliminate it, based on any criteria. For BAO_MIN in particular, this has significant consequences. In experiments done on hyperspectral data similar to the one described in the original research when we applied BAO_MIN we obtained a band subset equal to approximately 20% of the original bands. Moreover, many of the bands formed large contiguous intervals. A first approach would be to compact these intervals through an artificial transform (either averaging or using any other type of weighting scheme). While this does not constitute the focus of our paper we note that in our experiments, weighted averages significantly reduced the spectral angle compared with both the BAO_MIN and BAO_MAX.

A more attractive approach is provided by the *Floating Feature Selection* technique described in [8]. We have adapted the technique in the algorithm described in Table 2. We note that compared with BAO, the *Floating Band Selection* algorithm (FBS) is able to eliminate bands. After a band is added (Step 6), we check to see if elimination of any band from B_1 will in fact increase the angle. If that is the case we select the band whose elimination would result in the largest angle and remove it from B_1 . The algorithm returns to Step 3 and seeks another band to add. We note that the complexity of the new method is not significantly different than that of BAO, the removal step being in fact comparable with the addition one. We also note that as with BAO, two different algorithms FBS_MIN and FBS_MAX can be constructed, based on the initial choice of bands.

Table 3. FBS_MAX (Floating Band Selection – Maximum Initial Difference)

<p>Given two vectors \mathbf{x} and \mathbf{y} of size n</p> <p>Step 1. Find i and j between 1 and n with $[i, j] = \arg \max_{\substack{1 \leq k_1 \leq n \\ 1 \leq k_2 \leq n \\ k_1 \neq k_2}} d(\mathbf{x}_{[k_1, k_2]}, \mathbf{y}_{[k_1, k_2]})$</p> <p>Step 2. $B_1 = \{i, j\}$</p> <p>Step 3. Find j between 1 and n such that with $j = \arg \max_{k \notin B_1} d(\mathbf{x}_{[B_1, k]}, \mathbf{y}_{[B_1, k]})$</p> <p>Step 4. If $d(\mathbf{x}_{[B_1, j]}, \mathbf{y}_{[B_1, j]}) \leq d(\mathbf{x}_{B_1}, \mathbf{y}_{B_1})$</p> <p style="padding-left: 2em;">Step 5. Then Stop</p> <p style="padding-left: 2em;">Step 6. Else</p> <p style="padding-left: 4em;">Step 7. $B_1 = B_1 \cup \{j\}$</p> <p style="padding-left: 4em;">Step 8. Find i such that $i = \arg \min_{k \in B_1} d(\mathbf{x}_{B_1 \setminus \{k\}}, \mathbf{y}_{B_1 \setminus \{k\}})$</p> <p style="padding-left: 4em;">Step 9. If $d(\mathbf{x}_{B_1 \setminus \{i\}}, \mathbf{y}_{B_1 \setminus \{i\}}) > d(\mathbf{x}_{B_1}, \mathbf{y}_{B_1})$ then $B_1 = B_1 \setminus \{i\}$</p> <p style="padding-left: 4em;">Step 10. Go to Step 3.</p>

The above algorithm focuses on only two spectra. However, in most problems, we are dealing with sets of spectra. FBS can be modified for such approaches. Given a target t and a set of undesired signatures x^1, x^2, \dots, x^m , the algorithm (titled *FBS_Clique*) replaces the equation in step 3 by one of the following two formulas for MAX and MIN respectively:

$$[i, j] = \arg \max_{\substack{1 \leq k_1 \leq n \\ 1 \leq k_2 \leq n \\ k_1 \neq k_2}} \min_{1 \leq k_3 \leq m} d(\mathbf{t}_{[k_1, k_2]}, \mathbf{x}_{[k_1, k_2]}^{k_3}) \quad (6)$$

$$[i, j] = \arg \min_{\substack{1 \leq k_1 \leq n \\ 1 \leq k_2 \leq n \\ k_1 \neq k_2}} \min_{1 \leq k_3 \leq m} d(\mathbf{t}_{[k_1, k_2]}, \mathbf{x}_{[k_1, k_2]}^{k_3}) \quad (7)$$

Similar changes need to be done for the formula computed in the Add-On stage (Step 4.) and in the Removal stage (Steps 8-9). We note that such approach is similar to the one described in [7] as the Minimum Distance Method. We note however that, in the light of the discussion at the end of the previous section, FBS is intended as an enhancement to BAO_MIN as a way to reduce the number of bands, while increasing the angle between the spectra. As such, in the experiments section we have tested on the FBS_MIN.

4. EXPERIMENTAL RESULTS

To test the proposed algorithms we have taken the following two approaches:

4.1 Angle Maximization

We first investigated how the dynamicity of FBS impacts the overall objective of angle maximization. The first data set is a Hyperspectral Digital Imagery Collection Experiment (HYDICE) image corresponding to an urban scene. The data is 16 bit, reflectance values organized in 210 bands spanning the 400 to 2500nm range. The urban data set is one of the standard data sets used for testing dimensionality reduction algorithms and is freely available with Hypercube [12]. A color composite image of the datacube is show in Fig. 2a. The scene (generically titled URBAN) contains various classes including trees, grass, other vegetation, asphalt, concrete, soil, rooftops. The most representative classes are presented in Fig. 2b. Spectra for each class were obtained also from the Hypercube page. We note that the eight spectra display a wide range of variability. An initial preprocessing step was followed that resulted in elimination of band bands and yielded spectra using 157 bands.

We next computed the spectral angle for each pair of spectra. We applied BAO_MAX, BAO_MIN and FBS_MIN for each pair and computed the resulting angles (see Table 4). The maximum angle for each pair is highlighted with Bold fonts. As indicated by previous literature both BAO versions provide increased angles, with BAO_MAX resulting in significantly large angles. Comparatively, FBS_MIN while starting from the smallest angle is able to select subsets of bands that produced angles similar to BAO_MAX. Moreover, in several instances, the angles produced by the new method are larger than BAO_MAX.

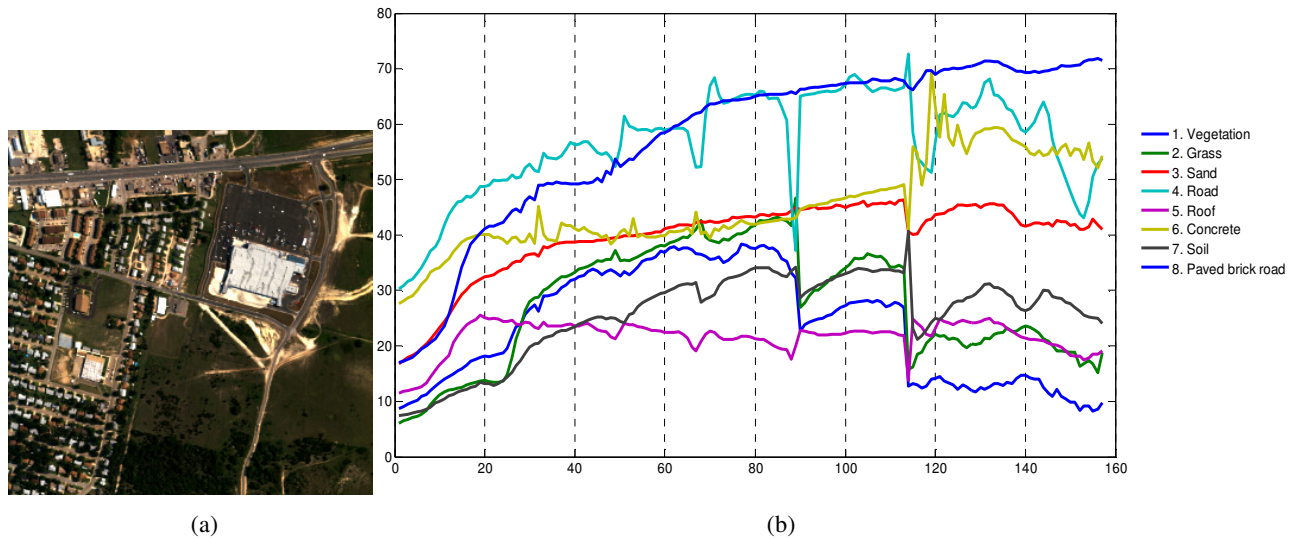


Figure 2. Urban Data Set a) Color composite image, b) spectra extracted from the image

Table 4. Results on the eight urban spectra. Values correspond to the angle obtained between spectra i (row) and spectra j (column).

	2	3	4	5	6	7	8	2	3	4	5	6	7	8	
REGULAR								BAO_MAX							
1	0.161	0.385	0.368	0.389	0.506	0.372	0.450	0.502	0.673	0.732	0.647	0.792	0.690	0.783	
2		0.291	0.295	0.349	0.418	0.243	0.334		0.475	0.788	0.683	0.639	0.619	0.557	
3			0.090	0.149	0.141	0.149	0.100			0.365	0.407	0.270	0.448	0.289	
4				0.140	0.177	0.176	0.163				0.492	0.423	0.607	0.543	
5					0.183	0.284	0.234					0.349	0.779	0.596	
6						0.257	0.154						0.539	0.459	
7							0.137							0.327	
FBS_MIN								BAO_MIN							
1	0.478	0.659	0.694	0.642	0.775	0.676	0.775	0.384	0.643	0.608	0.584	0.751	0.583	0.744	
2		0.485	0.749	0.678	0.683	0.432	0.535		0.423	0.607	0.627	0.621	0.432	0.511	
3			0.329	0.360	0.269	0.448	0.264			0.253	0.305	0.235	0.360	0.258	
4				0.348	0.368	0.596	0.526				0.348	0.345	0.467	0.430	
5					0.347	0.737	0.552					0.307	0.621	0.467	
6						0.611	0.465						0.486	0.392	
7							0.318							0.277	

Next we analyze the number of bands produced by each of the methods. We note that in case of FBS we have controlled the level to which band removal is performed. At the very least, removal should not be allowed when B_j is of size three or less, since this would mean that the MIN criteria is invalidated by the selection of a pair with a larger angle. Both Table 4 and 5 include FBS results that do not remove bands when the subset is smaller than five. Table 5 provides the final number of bands. We see that while BAO_MAX usually produces 2-4 bands (with few cases above that), BAO_MIN varies significantly with the number of bands ranging from 5 to 36. Compared to that, FBS_MIN has the lower limit provided by the subset size threshold chosen and is not significantly increasing above that. We note however that FBS_MIN is consistently producing more bands than BAO_MAX.

To better understand how the subset size threshold affects the FBS result we have varied the subset size from 3 to 20 and applied the algorithm to the every pair that included the first spectra (Vegetation). The resulting seven sequences of data are available in Fig. 3a. The graph plots the number of bands produced by FBS_MIN versus the subset size. The figure suggests that FBS is unlikely to produce more bands than BAO_MIN and, in fact is able to reduce the subset significantly.

Table 5. Urban data set spectra. Number of bands produced by each method

	2	3	4	5	6	7	8	2	3	4	5	6	7	8	2	3	4	5	6	7	8		
BAO_MAX								BAO_MIN								FBS_MIN							
1	3	4	3	4	4	3	4	36	7	12	22	7	26	8	5	5	6	7	5	5	5		
2		7	5	4	8	2	2		15	12	21	12	5	8		8	5	8	8	5	7		
3			2	2	4	5	7			8	8	16	10	15			5	5	5	5	6		
4				2	2	4	4				5	7	18	17				5	5	5	5		
5					2	3	3					13	9	17					5	5	5		
6						7	5						15	15						8	6		
7							4							10							5		

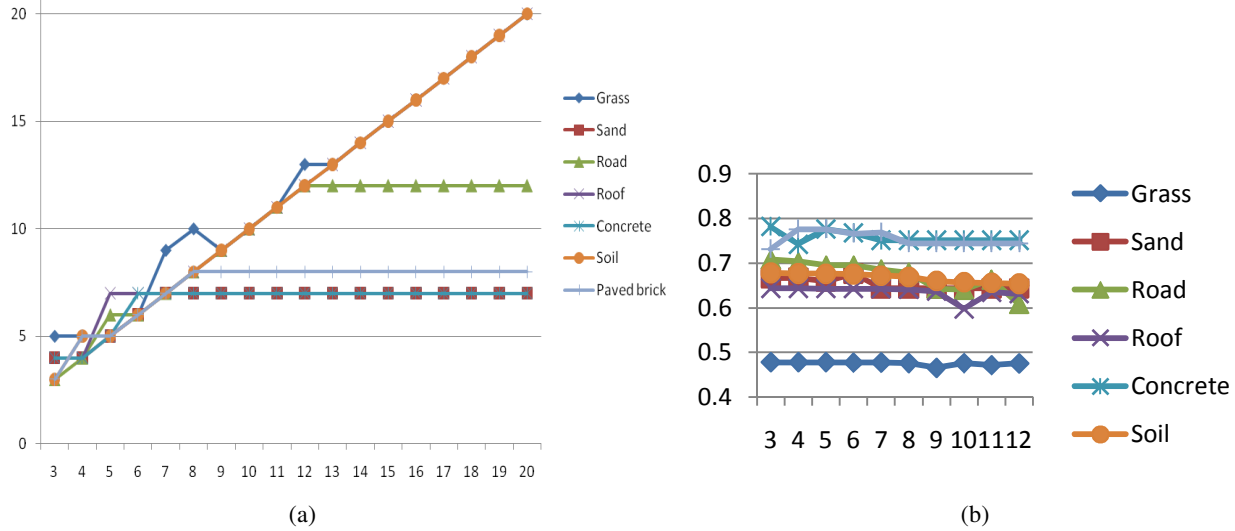


Figure 3. Urban Data Set FBS_MIN a) Number of bands as function of the minimum subset size, b) resulting spectral angle as function of minimum subset size

More important we note that strong stability of the resulting spectral angle values. Figure 3b plots the resulting spectral angle for FBS_MIN as the minimum size for the subset is varied from 3 to 12. While slight decreases are noted for some pairs, no significant change is noted. As with Figure 3a, FBS_MIN was run on pairs of spectra where one was Vegetation and the other each of the seven remaining spectra.

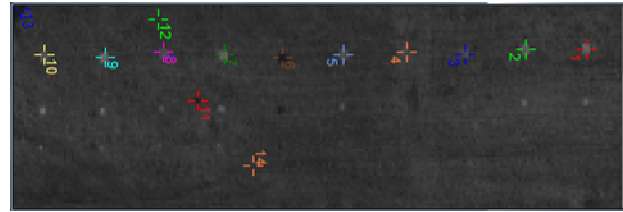
4.2 Target Detection

In Section 3 we expanded the FBS algorithm to a novel technique that looks at the minimum angle between a target spectra and a set of undesired spectra. To understand how such algorithm would work we have used as second data set is a Hyperspectral Digital Imagery Collection Experiment (HYDICE) image corresponding part of the Forest Radiance set. The data is 16 bit, reflectance values organized in 210 bands spanning the 400 to 2500nm range and collected with a spatial resolution of 1.5m. The Forest Radiance data is provided by the Spectral Information Technology Application Center (SITAC), and is often found in published research involving targets. Figure 4a provides a view of a sub scene of the large data, whereas Figure 4b shows the color composite image of the subscene, while Fig 4b shows a visible band view of the subscene area that was employed in our experiments. The area presents a special advantage through 30 man made panels placed in 3 rows on the ground, each of the 10 columns contains a different material, while each of the row contains panels of different sizes (3m by 3m, 2m by 2m, and 1m by 1m respectively). The sizes mean that the third row panels are basically smaller than the spatial resolution, and thus, the pixels covering them will have to be inherently mixed.

We extracted spectra for each of the ten pane types by manually identifying the centers of the largest panels. To these 10 spectra we also collected 4 additional ones at various locations on the scene corresponding to the ground, grass, a fragment of forest and an artifact. An initial preprocessing step was followed that resulted in elimination of band bands and yielded spectra using 149 bands. The graph for all fourteen spectra is visible in Figure 5. We note that unlike the urban scene, the spectra display a high level of similarity indicating that large angles will be unlikely to be produced. Next, we applied spectral angle mapping using all bands, as well as the bands produced by MDM and FBS_Clique. In each case, following the computation of the angles for each pixel, all values that were higher than a certain threshold were marked as zero to enhance visibility. The threshold was chosen as the minimum angle between the target and the undesired signatures. The results are inconclusive, as in the case of some targets both MDM and FBS_Clique outperform directly the use of full band sets, while in others, they introduce additional false positives. As representative results we provide the angle maps for the first, third and tenth column of panels (see Figure 6). This lack of consistency can be explained by the small number of spectra we employed. A thorough analysis is required to validate our approach. In that case, the target should be represented by additional spectra, while the number of non desired signatures may also need to be increased.



(a)



(b)

Figure 4. Forest Radiance Data Set a) Color composite image of the subszene with the area that was processed highlighted b) area that was processed with 14 spectra chosen. The image includes 30 panels organized in 3 rows, each row has a different panel size.

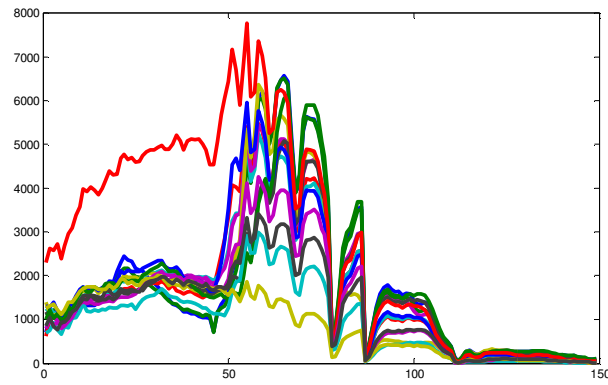


Figure 5. Forest Radiance Data Set. Plot of the fourteen spectra collected for further processing.

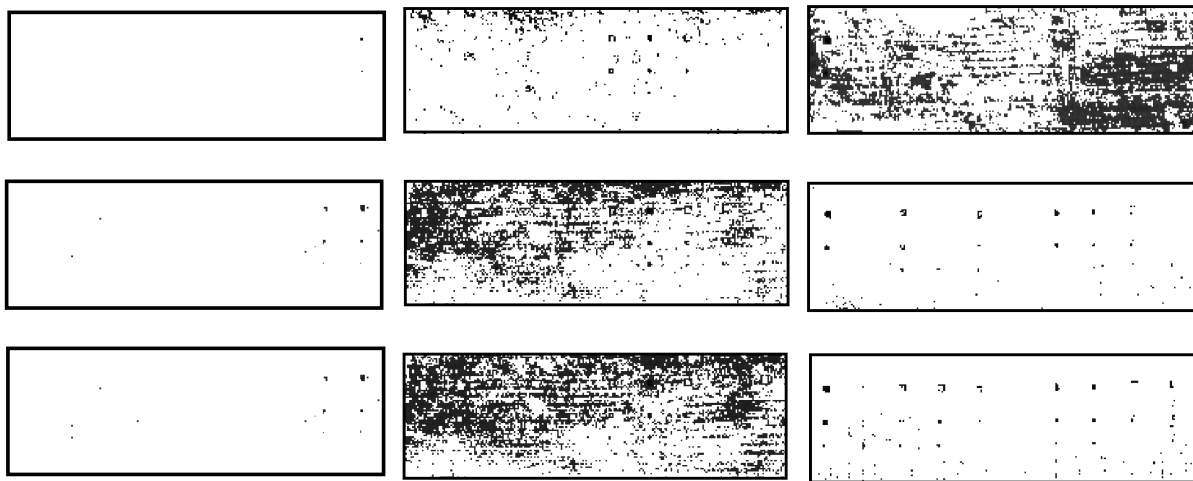


Figure 6. Forest Radiance Data Set. Target detection results for panels on columns 1, 3, and 10 (right to left)

5. CONCLUSIONS

We introduced a new technique that enhanced the separation of spectra through iteratively selecting the bands that increase the distance between spectra. Compared with previous approaches that focus only on band addition to the selected subset, the Floating Band Selection approach is able to backtrack its steps and eliminate bands which would reduce the overall distance. While not explicitly indicated, the algorithm can be easily modified to work with other measures than the spectral angle. We further expanded the algorithm to be employed for target detection. In each case, the experimental results matched or improved upon the Band Add On counterparts. Several concerns remain for expansion of algorithm usability. As with previous algorithms FBS is not optimal, and the subset of bands varies based on internal parameters. An exhaustive investigation of the optimal solution is desired and is planned using high performance computing. Second, in case of groups of spectra, the algorithm fails to maintain consistency. We intend to investigate various solutions including addition of more representatives for the target or redevelopment of the algorithm to focus on a multi-class environment (compared to the two class problem).

6. ACKNOWLEDGEMENTS

The author's work was supported through Montclair State University Faculty Scholarship Program 2008-2013. This material is based in part upon work supported by the National Science Foundation under Grant Number CNS-0922644. Any opinions, findings, and conclusions or recommendations expressed in this material are those of the author(s) and do not necessarily reflect the views of the National Science Foundation.

REFERENCES

- [1] C.C. Slama, C. Theurer, and S.W. Henriksen, *Manual of photogrammetry*, American Society of Photogrammetry Falls Church, Virginia, 1980.
- [2] R.L. Kettig and D.A. Landgrebe, "Classification of multispectral image data by extraction and classification of homogeneous objects," *IEEE Transactions on Geoscience Electronics*, vol. 14, 1976, pp. 19-26.
- [3] D.A. Landgrebe, *Signal theory methods in multispectral remote sensing*, Wiley-InterScience, 2003.
- [4] C.I. Chang, *Hyperspectral data exploitation: theory and applications*, Wiley-Blackwell, 2007.
- [5] R. Lu and Y.R. Chen, "Hyperspectral imaging for safety inspection of food and agricultural products," *Proceedings of SPIE*, 1999, p. 121.
- [6] S.B. Serpico, M. D'Inca, F. Melgani, and G. Moser, "Comparison of feature reduction techniques for classification of hyperspectral remote sensing data," *Proceedings of SPIE*, 2003, p. 347.
- [7] N. Keshava, "Distance metrics and band selection in hyperspectral processing with applications to material identification and spectral libraries," *IEEE Transactions on Geoscience and Remote Sensing*, vol. 42, 2004, pp. 1552-1565.
- [8] P. Somol, P. Pudil, J. Novoviková, and P. Paclik, "Adaptive floating search methods in feature selection," *Pattern Recognition Letters*, vol. 20, 1999, pp. 1157-1163.
- [9] R.H. Yuhas, A.F.H. Goetz, and J.W. Boardman, "Discrimination among semi-arid landscape endmembers using the spectral angle mapper (SAM) algorithm," *Summaries of the Third annual JPL airborne geoscience workshop*, Pasadena, CA: JPL Publication, 1992, pp. 92-14,147.
- [10] Y. Sohn and N.S. Rebello, "Supervised and unsupervised spectral angle classifiers," *Photogrammetric Engineering and Remote Sensing*, vol. 68, 2002, pp. 1271-1282.
- [11] S.A. Robila and N.A. Senedzuk, "Grid computing for hyperspectral data processing," *Next-Generation Spectroscopic Technologies*, C.D. Brown, M.A. Drury, and J.P. Coates, eds., SPIE, 2007, p. 67650A.
- [12] R. Pazak, *HyperCube Users' Manual*, Topographic Engineering Center Internal Report, 2002.